

Numerical investigation of angle of attack profile on propulsion performance of an oscillating foil

Qing Xiao^a, Wei Liao^{b,*}

^a Department of Naval Architecture and Marine Engineering, University of Strathclyde, Glasgow G4 0LZ, UK

^b Department of Mathematics and Statistics, Old Dominion University, Norfolk, VA 23529, USA

ARTICLE INFO

Article history:

Received 26 August 2009

Received in revised form 3 March 2010

Accepted 13 April 2010

Available online 22 April 2010

Keywords:

Pitching/plunging oscillation

Propulsion performance

Effective angle of attack

Cosine profile

ABSTRACT

Effects of effective angle of attack (AOA) profile on an oscillating foil thrust performance are studied using a computational method. The foil is subject to a combined pitching/plunging motion with effective AOA satisfying a harmonic cosine function. To achieve this, either the pitching or plunging motion is modified from the conventional harmonic sinusoids. Investigations are performed over a series of Strouhal numbers (St), three maximum effective angles of attack and three different phase angles between pitching and plunging. It is shown that the degradation of thrust force and efficiency with sinusoidal pitching/plunging oscillation, at higher St , is effectively alleviated or removed when the AOA is imposed as a cosine profile. The improvement is more significant for the phase angle being different from 90° . A better performance is obtained with the imposed modification on pitching motion. The stronger reversed Von Karman vortex wake associated with leading-edge vortex development is observed with the modified motions, which is believed to induce the improved thrust performance.

© 2010 Elsevier Ltd. All rights reserved.

1. Introduction

Oscillating airfoil with pure pitching, pure plunging or combination of both motions have potential applications in the design of high efficient Micro Air Vehicle (MAV) and Autonomous Underwater Vehicle (AUV). Numerous experimental and numerical studies have investigated the flows around an oscillating foil [1–13,16,17]. It is generally accepted that the wake structure downstream of the trailing edge plays a significant role on the forces generated by an oscillating foil. At a low oscillating frequency, the wake has a von Karman vortex street which consists of two rows of vortices. The upper row of vortices in the wake rotates clockwise and the lower row of vortices rotates counter clockwise. This causes the momentum deficit in the wake compared to the upstream flow and thus a drag force is generated. On the other hand, at a relatively high oscillating frequency, the wake consists of two rows of vortices with upper row of vortices rotating counter clockwise and the lower row of vortices rotating clockwise. The time-mean velocity profile at the trailing edge indicates a momentum surplus in the wake and then a thrust is generated as a consequence.

Apart from the wake structure, some past experimental and numerical work has studied the kinetics and flow characteristics of oscillating foils including the lift, drag and propulsion efficiency. Typical experimental studies include Read et al. [1], Hover et al. [2],

Anderson [3], Anderson et al. [4], Lai and Platzer [8] and Koochesfahani [11]. A number of numerical simulations were conducted by Lewin and Haj-Hariri [5], Tuncer and Platzer [6], Young and Lai [7], Isogai et al. [9] Yang et al. [10], Sarkar and Venkatraman [12,13], and Xiao and Liao [16,17]. The general conclusion from the existing investigations is that the thrust and propulsive efficiency strongly depends on the various combinations of oscillating parameters. They are the amplitudes of pitching/plunging motions (θ_0 and h_0), the phase angle difference between these two motions (ψ) and the non-dimensional oscillating frequency, *i.e.* reduced frequency (k) or the Strouhal number (St). Here, k and St are defined as $k = \omega c / 2U_\infty$ and $St = fA / U_\infty$, respectively, where c is the chord length of airfoil, ω is the angular frequency, U_∞ is the free-stream velocity, A is the characteristic width of the wake $A = 2h_0$ and f is the oscillating frequency. For an oscillating foil with given amplitudes and phase angle difference, the oscillating frequency has a considerable effect on the thrust generation. At a low frequency, the thrust coefficient increases with increasing St . However, when St is increased beyond a certain value, the thrust decreases with further increasing of St .

Although the effect of St on an oscillating foil is well observed by previous studies, the relation between effective AOA and degradation of thrust performance at higher St has not drawn much attention. Only two experimental studies were reported by Read et al. [1] and Hover et al. [2]. From their measurements of lift, thrust forces and torque on a NACA0012 oscillating foil, Read et al. [1] found that at a high St , the reduction of thrust coefficient is caused by the degradation of effective angle of attack $\alpha(t)$. They further demonstrated

* Corresponding author. Tel.: +1 757 683 6001x5035; fax: +1 757 683 3885.
E-mail addresses: qing.xiao@strath.ac.uk (Q. Xiao), wliao@odu.edu, lwpynus@gmail.com (W. Liao).

that with the introduction of properly designed higher order harmonics in the plunging motion, the degradation extent can be improved, and thus the thrust coefficient is recovered. Hover et al. [2] extended the work of Read et al. [1] with several different angle of attack profiles including a square wave, a symmetric sawtooth wave and a cosine function. In terms of high thrust with reasonable high efficiency, cosine AOA is found to be the best among three cases. Although the linkage between the effective AOA profile and thrust is well established, there appears to be a lack of systematic investigation on how to modify the effective AOA to achieve high thrust performance and on the flow mechanism behind it.

The objective of this study is to investigate numerically the thrust force, input power and efficiency of an oscillating NACA0012 airfoil undergoing a modified non-sinusoidal pitching or plunging motion with a resultant effective AOA of the cosine profile. Computations are conducted at a constant Reynolds number (based on free-stream velocity and the chord length of the airfoil) of 2.2×10^4 , and with three different maximum AOA of $\alpha_{\max} = 10^\circ, 15^\circ$ and 20° , three phase angles $\psi = 80^\circ, 90^\circ$ and 100° , and a series of the Strouhal numbers from 0.1 to 0.7. The foil pitches at one third chord location. Different from previous experimental studies [1–2], our attention is not only limited to the modification on plunging motion, but also extended to that on pitching motion, which is shown later to be a more efficient technique than plunging modification. The wake structure caused by the amended oscillation and surface pressure distribution, which is not easily measured in the experiment, will also be examined to explore the flow mechanism behind the supposed modifications.

2. Computational approach

2.1. Governing equations

To simulate the time-dependent viscous flow around an oscillating NACA0012 airfoil, we solve the unsteady two-dimensional Navier–Stokes (NS) equations with a compressible flow solver at a low free-stream Mach number as conducted in our previous work [17].

The governing equations for unsteady compressible flows are expressed as follows:

$$\frac{\partial}{\partial t} \int_V \mathbf{W} dV + \int_S (\mathbf{F}_c - \mathbf{F}_d) \cdot \mathbf{n} dS = 0 \quad (1)$$

where V denotes a control-volume with closed boundary surface S , and \mathbf{n} is the outward unit normal vector on S . The vector \mathbf{W} contains the conservative variables.

$$\mathbf{W} = \{\rho, \rho u, \rho v, \rho w, \rho E\}^T \quad (2)$$

where ρ is the density, u , v , and w are the three Cartesian velocity components and E is the specific total energy of the flow, given by

$$E = e + \frac{1}{2}(u^2 + v^2 + w^2) \quad (3)$$

where e is the internal energy.

The flux tensor in Eq. (1) consists of the inviscid convective fluxes \mathbf{F}_c and the diffusive fluxes \mathbf{F}_d . The convective fluxes \mathbf{F}_c are expressed in terms of the relative velocity $\mathbf{u} - \mathbf{u}_b$, i.e.

$$\mathbf{F}_c = \begin{Bmatrix} \rho(u - u_b) & \rho(v - v_b) & \rho(w - w_b) \\ \rho u(u - u_b) + p & \rho u(v - v_b) & \rho u(w - w_b) \\ \rho v(u - u_b) & \rho v(v - v_b) + p & \rho v(w - w_b) \\ \rho w(u - u_b) & \rho w(v - v_b) & \rho w(w - w_b) + p \\ \rho H(u - u_b) & \rho H(v - v_b) & \rho H(w - w_b) \end{Bmatrix} \quad (4)$$

where $\mathbf{u}_b = (u_b, v_b, w_b)^T$ is the grid velocity vector and $H = E + \frac{p}{\rho}$ is the specific total enthalpy. The diffusive fluxes due to the viscous shear stresses and thermal diffusion can be written as

$$\mathbf{F}_d = \begin{Bmatrix} 0 & 0 & 0 \\ \tau_{xx} & \tau_{xy} & \tau_{xz} \\ \tau_{yx} & \tau_{yy} & \tau_{yz} \\ \tau_{zx} & \tau_{zy} & \tau_{zz} \\ \theta_x & \theta_y & \theta_z \end{Bmatrix} \quad (5)$$

Here, $\tau_{\alpha\beta}$ with $\alpha, \beta \in \{x, y, z\}$ is the stress tensor and

$$\begin{aligned} \theta_x &= u\tau_{xx} + v\tau_{xy} + w\tau_{xz} - q_x \\ \theta_y &= u\tau_{xy} + v\tau_{yy} + w\tau_{zy} - q_y \\ \theta_z &= u\tau_{xz} + v\tau_{yz} + w\tau_{zz} - q_z \end{aligned} \quad (6)$$

In a Newton–Fourier fluid, the viscous shear stresses and heat fluxes can be defined as

$$\tau_{\alpha\beta} = \mu(\partial_\alpha u_\beta + \partial_\beta u_\alpha) - \frac{2}{3}\mu\delta_{\alpha\beta}\partial_\gamma u_\gamma \quad (7)$$

$$q_\alpha = -k\partial_\alpha \Theta \quad (8)$$

with the dynamic viscosity μ , the thermal conductivity k , and the temperature Θ . The coefficient of dynamic viscosity μ is obtained by the Sutherland’s formula [17].

2.2. Numerical methods

The governing Eq. (1) is solved based on structured multiblock grids using a finite-volume method. The arbitrary Lagrangian–Eulerian method is adopted to allow for the moving boundary due to the motion of airfoil. It is here achieved by defining fluxes relative to the surface movement of the control-volume. Therefore, the convective fluxes are expressed in terms of the relative velocity $\mathbf{u} - \mathbf{u}_b$ as shown in Eq. (4). A second-order central-difference scheme with artificial dissipation as proposed by Jameson et al. [18] is applied for spatial discretization. The artificial dissipative terms are made up of a blend of second-order and fourth-order differences to provide third-order dissipation in smooth flow region [18]. The dual-time method proposed by Jameson [19] is used to perform time-accurate calculations. A second-order accurate fully implicit scheme is then used to discretize the derivative of the physical time. To accelerate the convergence of the solution in pseudo-time, Runge–Kutta multi-stage time integration with the multigrid strategy [18] is utilized. The multiblock structure in the current solver provides the natural basis for the parallel implementation. Information exchange for flow computation on multiblock grids using multiple CPUs is applied through the Message Passing Interface (MPI) protocol. The present numerical method and code have been extensively verified for unsteady compressible viscous flows by Xiao et al. [14–15] and incompressible asymmetric NACA0012 pitching flow in Xiao and Liao [17].

2.3. Parameters relevant to combined pitching/plunging motion of a foil

The combined sinusoidal motion of a pitching and plunging foil is expressed as:

$$h(t) = h_0 \sin(\omega t) \quad (9)$$

$$\theta(t) = \theta_0 \sin(\omega t + \psi) \quad (10)$$

The instant effective angle of attack $\alpha(t)$ is composed of pitching angle $\theta(t)$ and plunging induced angle of attack $(-\arctan(\frac{\dot{h}(t)}{U_\infty}))$ as a result of translational velocity of the airfoil and therefore defined as:

$$\alpha(t) = -\arctan\left(\frac{\dot{h}(t)}{U_\infty}\right) + \theta(t) \quad (11)$$

The nominal angle of attack is irrelevant of instant time and expressed by

$$\alpha_0 = -\arctan\left(\frac{\omega h_0}{U_\infty}\right) + \theta_0 \quad (12)$$

For phase angle difference ψ of 90° and small St , α_0 is equal to the maximum angle of attack α_{\max} while they are different when $\psi \neq 90^\circ$ or at large St .

The parameters related to propulsion performance of an oscillating airfoil are thrust coefficient (C_t), input power coefficient (C_{ip}) and propulsion efficiency (η). The mean thrust coefficient per unit span length during one oscillation period is defined as

$$C_t = \frac{\bar{F}}{\frac{1}{2}\rho U_\infty^2 c} \quad (13)$$

where \bar{F} is the time-averaged value of the force component $X(t)$ in the x direction and is obtained by integration of the instant force

$$\bar{F} = \frac{1}{T} \int_0^T X(t) dt \quad (14)$$

where T is the oscillation period.

The mean input power coefficient is expressed as

$$C_{ip} = \frac{\bar{P}}{\frac{1}{2}\rho U_\infty^3 c} \quad (15)$$

where the mean input power is calculated by

$$\bar{P} = \frac{1}{T} \left[\int_0^T Y(t) \frac{dh(t)}{dt} dt + \int_0^T M(t) \frac{d\theta(t)}{dt} dt \right] \quad (16)$$

where $Y(t)$ is the force component in y direction and $M(t)$ is the pitching moment.

The overall propulsion efficiency is expressed by

$$\eta = \frac{C_t}{C_{ip}} \quad (17)$$

3. Results and discussions

3.1. Code validation

Prior to conducting a detailed computation, we performed the grid and domain independence tests along with a series of validation cases to verify the capability of current compressible code for modeling near incompressible flow at a low free-stream Mach number. Note that the validation for a purely pitching foil has been done in our previous work [17]. Comparisons with existing experimental and computational results cover the predictions of time-mean forces, time-dependent force, and instant vortex structure.

3.1.1. Grid independence test

We first consider an experimental test case by Anderson et al. [4]. The foil oscillates in a coupled pitching/plunging motion around one third chord with a plunging amplitude $h_0 = 0.75$, a nominal angle of attack $\alpha_0 = 15^\circ$ and the phase difference between pitching and plunging $\psi = 90^\circ$. The far-stream Mach number is set to be 0.06.

A C-type mesh is used with 20 chords length extension in all directions, which has been examined by domain independence tests with different domain sizes. To assess grid independence, three different resolution meshes are used with a coarse mesh of 193×33 , a medium mesh of 385×65 and a fine mesh of 769×97 . The computed instant drag coefficient C_d ($C_d = -C_t$) and power coefficient C_{ip} variations in one oscillating period are shown in Fig. 1a and b with the Strouhal number fixed at $St_{TE} = 0.35$.

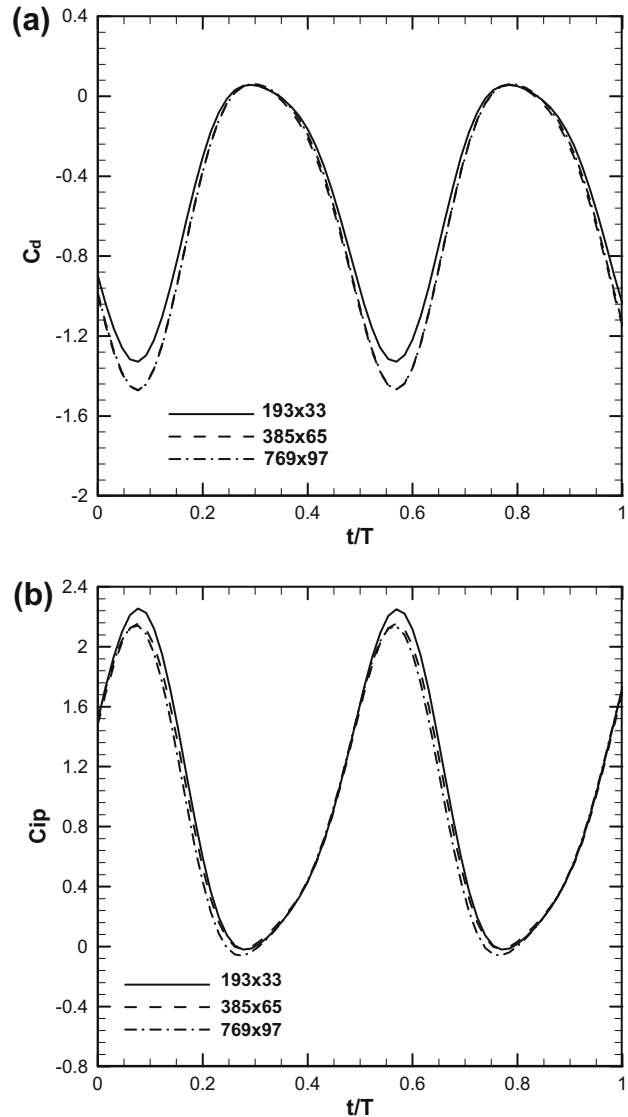


Fig. 1. Grid independence test for Anderson case with $h_0 = 0.75$, $\psi = 90^\circ$, $\alpha_0 = 15^\circ$ and $St_{TE} = 0.35$. (a) Instant drag coefficient. (b) Instant power coefficient.

($St_{TE} = fA_{TE}/U_\infty$, where A_{TE} is the excursion of the trailing edge) Comparison of the three results indicates no significant differences between the solutions on the medium mesh and those on the fine mesh. Therefore, the simulations presented in the following are conducted on the mesh of 385×65 unless otherwise stated.

3.1.2. Time-mean force

The aforementioned case conducted by Anderson et al. [4] has also been computed to validate the current code through the comparison of time-mean forces. Fig. 2a–c illustrate the predicted time-mean thrust coefficient, power coefficient and propulsion efficiency variation with St_{TE} along with the experimental data and nonlinear simulation of Anderson et al. [4] at Reynolds number ($Re = U_\infty c/\nu$) of 2×10^4 . In the present work, the computations are conducted using both the Euler and Navier–Stokes solver. As indicated in the figures, both computation and experiment present the increased thrust coefficient and power coefficient with increasing St_{TE} . For propulsion efficiency η , an optimal St_{TE} with the value of around 0.2–0.25 is found, at which the efficiency reaches the maxima.

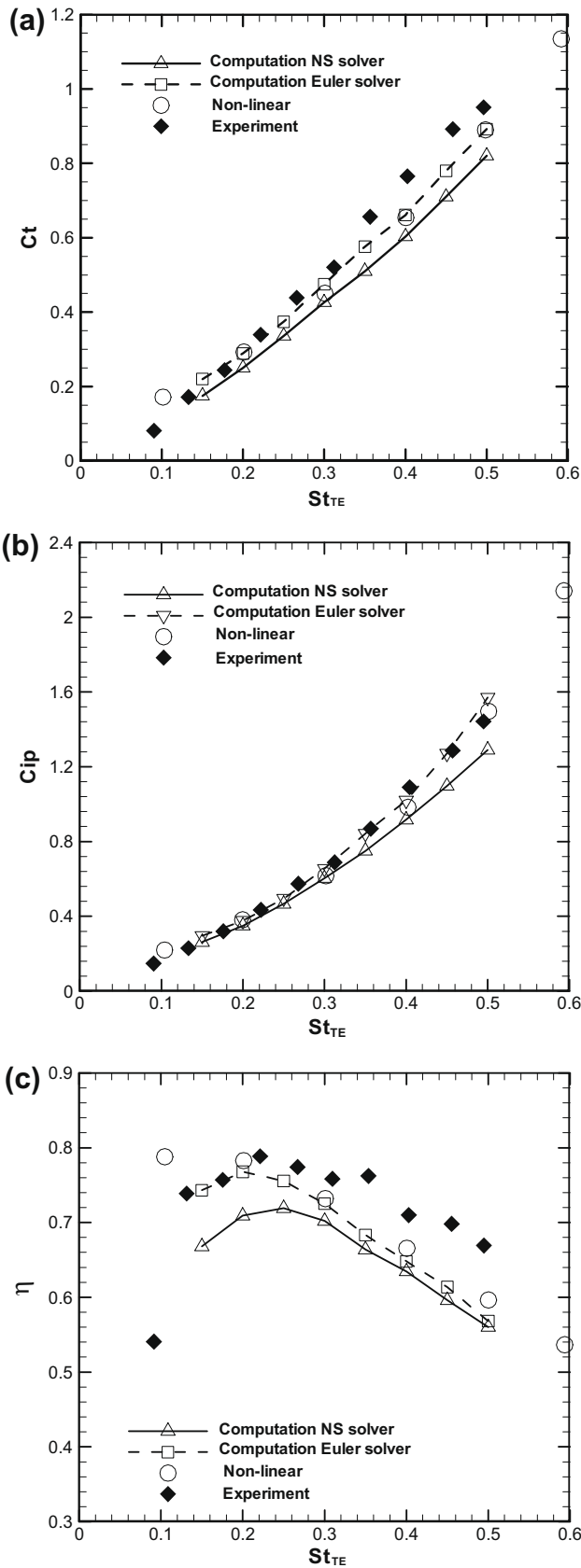


Fig. 2. Comparison of the present computation with the experiment and nonlinear simulation by Anderson et al. [4] with $h_0 = 0.75$, $\psi = 90^\circ$, $\alpha_0 = 15^\circ$ and $St_{TE} = 0.35$. (a) Thrust coefficient. (b) Power coefficient. (c) Propulsive efficiency.

In general, our Euler results agree very well with nonlinear data from Anderson et al. [4] as shown in Fig. 2a since both methods are inviscid based and satisfy the Kutta condition at the foil trailing edge. The thrust coefficients predicted by the NS solver are always smaller than those by the Euler solver which well reflects the effect of the viscosity on the C_t . For low St_{TE} , like $St_{TE} < 0.35$, where the flow field is dominated by the trailing edge vortices, the difference between the results of two solvers is small and both are close to the experiments. At higher Strouhal numbers, with the vortices shedding from leading edge, moving downstream and interfering with trailing vortices, C_t obtained by the NS solver deviates from those of the Euler and nonlinear solutions. In the meantime, all these numerical results underpredicted the thrust coefficients compared to the experiments, with the Euler and nonlinear results being closer to the experiments. The power coefficient plotted in Fig. 2b shows that the predicted C_{ip} from Euler and NS solver are in excellent agreement with nonlinear and experimental data for $St_{TE} < 0.35$. With further increasing of St_{TE} , the NS solutions underpredict C_{ip} in comparison with both the inviscid solutions and experimental results. Fig. 2c illustrates that the efficiency from the NS solver is generally lower than the Euler results and the experimental data of Anderson et al. [4] which is apparently caused by their discrepancy in C_t and C_{ip} .

Based on the above observations, it is seen that the present Euler solutions match the reported nonlinear inviscid solutions very well in terms of C_t , C_{ip} and η . The current NS solutions have reasonably lower C_t than the inviscid results, which in turn lead to a lower efficiency. An unusual observation is that the experimental results have better agreement with the inviscid solutions than the NS results although their predicted trends are consistent. Such discrepancy between experiments and the NS simulations on thrust coefficient has also been observed in many previous studies for flapping-foil cases such as Jones and Platzer [20], Liu and Kawachi [21], Ramamurti and Sandberg [22], and Young and Lai [23]. The potential sources of error have been explored as well. As pointed out in Refs. [20,22,23], the poor agreement at large St may be attributed to the inaccurate force measurement techniques employed in the experiment, based on the momentum theory. In the experiments, including Anderson et al. [4], the thrust is obtained by measuring the momentum deficit or surplus downstream of the body. This technique may cause errors when velocity measurements are taken at the plane not sufficiently far downstream of the oscillating body where the wake eddies are still coherent.

3.1.3. Time-dependent force

To validate the accuracy of the present solver for predicting time-dependent forces, we studied a pure plunging NACA0012 foil and compared the calculated instant drag coefficient C_d with computational results of Tuncer and Platzer [6]. To match their computation based on the fully turbulent assumption with Reynolds number of $Re = 2 \times 10^4$, we computed the flows using both the laminar flow solver and the turbulent flow solver with the Baldwin–Lomax turbulence model as they exploited. The current flow solver with the turbulence model has been used and validated in the previous compressible computations conducted by Liao et al. [24]. The comparison of the present results and those of Tuncer and Platzer [6] on instantaneous C_d are shown in Fig. 3 at a given reduced frequency $k = 3.94$ and amplitude of $h_0 = 0.075$. As clearly seen, the difference between turbulent and laminar results is negligible. The initial discrepancy between present computation and Tuncer and Platzer [6], due to the different initial fields imposed, gradually diminishes and excellent agreement between two results

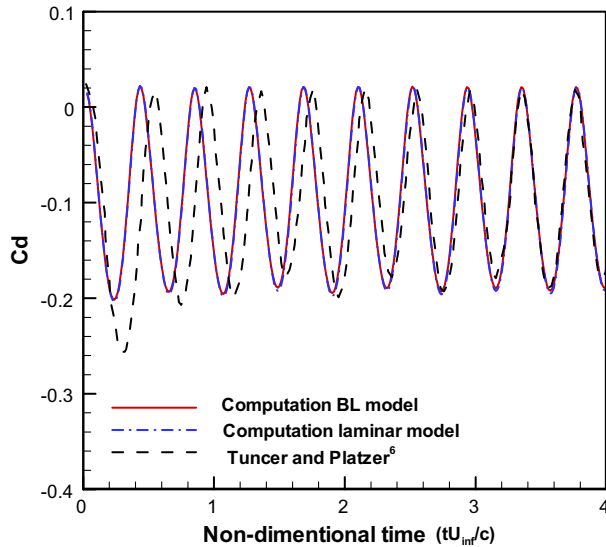


Fig. 3. Comparison of computed instant drag coefficient versus time with the results by Tuncer and Platzer [6] for $h_0 = 0.075$ and $k = 3.94$.

in terms of the amplitude and phase angle present since the non-dimensional time $t' = 3.2$, where $t' = tU_\infty/c$.

3.1.4. Vorticity structure

To validate the code capability for vortex structure capturing, we computed another test case from Anderson et al. [4]. The predicted wake structure is compared with the velocity visualization experimental results. The foil oscillates at a plunging amplitude of 0.25, a pitching amplitude of 15° , the phase difference of 90° and $St_{TE} = 0.36$. The DPIV plot from the experiment has been given in their Fig. 12a at the instant when the foil reaches the maximum positive position [4]. The corresponding computed result is illustrated in Fig. 4 showing the perturbation-velocity-vector plot where the perturbation-velocity is defined as $u' = u - U_\infty$.

A comparison of two figures shows that the reversed Kaman vortices structure in the wake is well captured by the present computation, three vortices are clearly observed and no leading-edge vortex appears. The positions of the core center of three vortices are in good agreement with experimental results.

In summary, the comparison of above systematically performed validation cases shows that the present simulations agree reason-

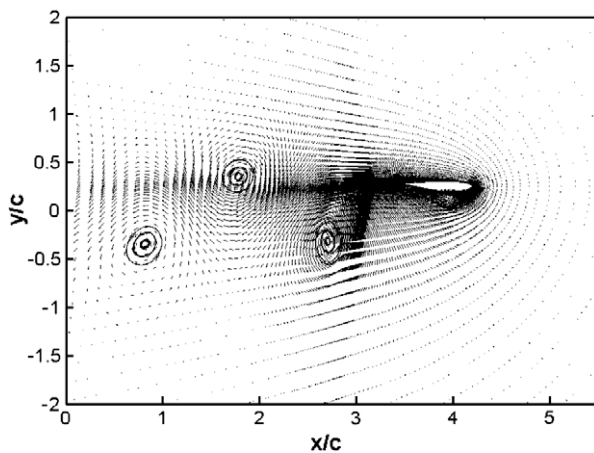


Fig. 4. Comparison of perturbation-velocity-vector plots from computational results and experiments (see Fig. 12a in Ref. [4]) and at maximum heave position of the foil with $h_0 = 0.25$, $\theta_0 = 15^\circ$, $\psi = 90^\circ$ and $St_{TE} = 0.36$.

ably well with the available experiments and simulations. Therefore, the current code shows good capability of simulating incompressible flows over an oscillating foil. All computations in the following study are conducted with the far-stream Mach number $Ma = 0.05$. The local Mach number at each point in the flow field is checked during computations and ensured to be less than 0.3 in the entire space and time domain in order to guarantee the near incompressible conditions.

3.2. Results for baseline oscillation

As mentioned earlier, simulations covered a wide range of St , three different maximum AOA, three phase angles with modified motion on pitching and plunging. For brevity, the term 'baseline' is used to refer to the case with the combined motion of sinusoidal harmonic pitching and plunging. We begin with presenting the results for the baseline case in this section.

3.2.1. Effect of maximum angle of attack

The thrust performance with the sinusoidal pitching/plunging motion for different α_{max} was first investigated for $h_0 = 1.0$ and $\psi = 90^\circ$. To achieve a given α_{max} , the pitching amplitude θ_0 is adjusted with a fixed plunging amplitude h_0 , phase angle difference ψ and oscillating frequency St . In Fig. 5a–c, the numerical results are shown for time-mean thrust coefficient, power coefficient and propulsion efficiency. As seen from Fig. 5a, for a fixed α_{max} , thrust coefficient initially increases with St before it reaches a critical value. Beyond this St , C_t decays with the further increasing of St . Also, it is noted that the larger α_{max} results in the higher critical St . The same trend is revealed in Fig. 5b for mean power coefficient. At the same St , with larger α_{max} like 20° , both thrust and power coefficients show the higher values than those with smaller α_{max} such as 10° and 15° . For $\alpha_{max} = 10^\circ$ and $\alpha_{max} = 15^\circ$, we observed the negative C_t at higher St indicating a drag-producing flow at this flow condition. The maximum St at which the flow changes from thrust producing to drag producing decreases significantly with decreasing α_{max} representing a faster degradation of propulsion performance at smaller α_{max} .

The propulsion efficiency versus St for two smaller maximum effective AOA $\alpha_{max} = 10^\circ$ and $\alpha_{max} = 15^\circ$, shown in Fig. 5c, illustrates a very slight increase of η at the initial stage followed by a fast decrease with increasing St . The critical St where efficiency starts dropping is larger for $\alpha_{max} = 15^\circ$ than that for $\alpha_{max} = 10^\circ$. Different from $\alpha_{max} = 10^\circ$ and $\alpha_{max} = 15^\circ$ cases, efficiency in the $\alpha_{max} = 20^\circ$ case remains a plateau at a relatively high level in a certain range of St ($0.3 < St < 0.6$) before it drops down.

3.2.2. Effect of phase difference between pitching and plunging

It was already known that, the phase difference between pitching and plunging ψ has a profound effect on the propulsion performance. We conduct the further investigation for two phase difference distinct from 90° , i.e. $\psi = 80^\circ$ and 100° at a fixed α_{max} of 15° and $h_0 = 1.0$.

The mean thrust coefficient, power coefficient and propulsion efficiency versus St are shown in Fig. 6a–c for $\psi = 80^\circ$, 90° and 100° with $\alpha_{max} = 15^\circ$ and $h_0 = 1.0$. As seen from these figures, the general trend of both $\psi = 80^\circ$ and $\psi = 100^\circ$ are similar to the results of $\psi = 90^\circ$. That is, C_t and C_{ip} increase with St before they decline with St and η keeps a relative constant then decay with St . The results for $\psi = 80^\circ$ are almost the same as those of $\psi = 100^\circ$ except for the C_{ip} curve. The most significant difference among these three cases is that the dropping of C_t , C_{ip} and η with $\psi = 80^\circ$ and $\psi = 100^\circ$ starts at a much smaller St than that with $\psi = 90^\circ$. This suggests that the most efficient propulsion performance should be at the phase difference ψ close to 90° . This is consistent with the previous experimental and numerical results [3,4,9]. Examinations of effec-

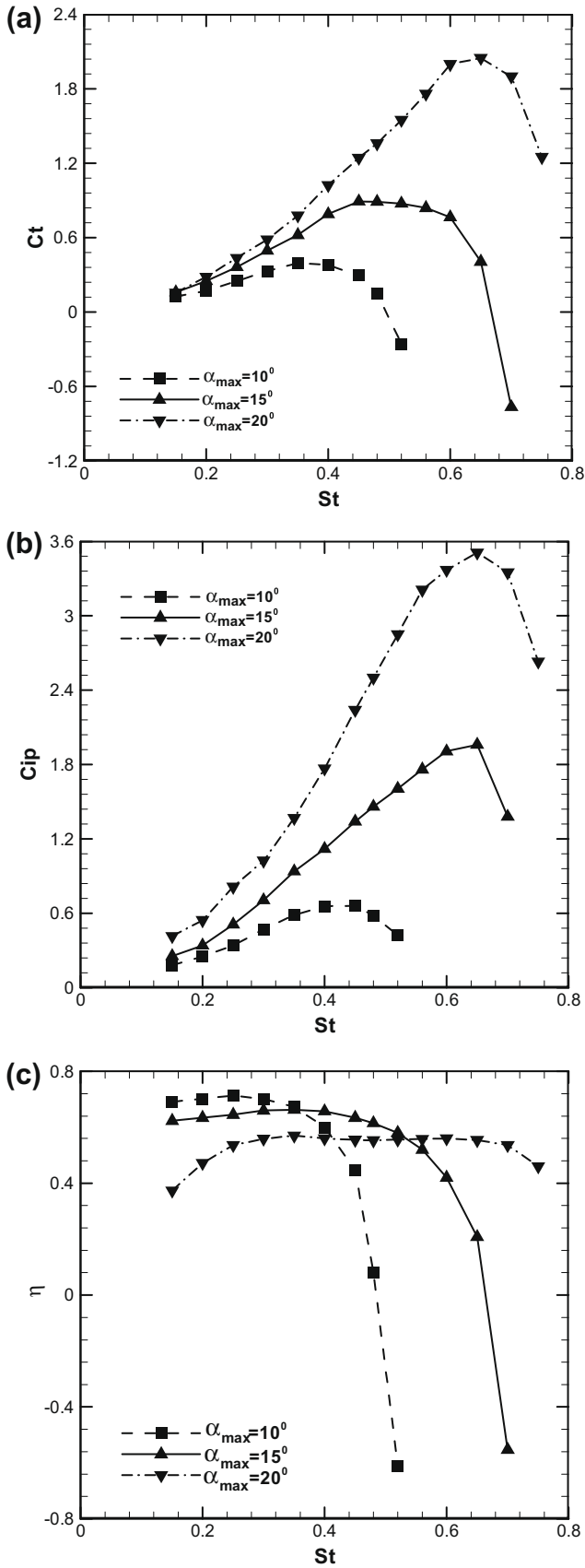


Fig. 5. Effect of α_{max} on the mean thrust coefficient, power coefficient and propulsion efficiency variation with St for the baseline case with $h_0 = 1.0$ and $\psi = 90^\circ$. (a) Thrust coefficient. (b) Power coefficient. (c) Propulsion efficiency.

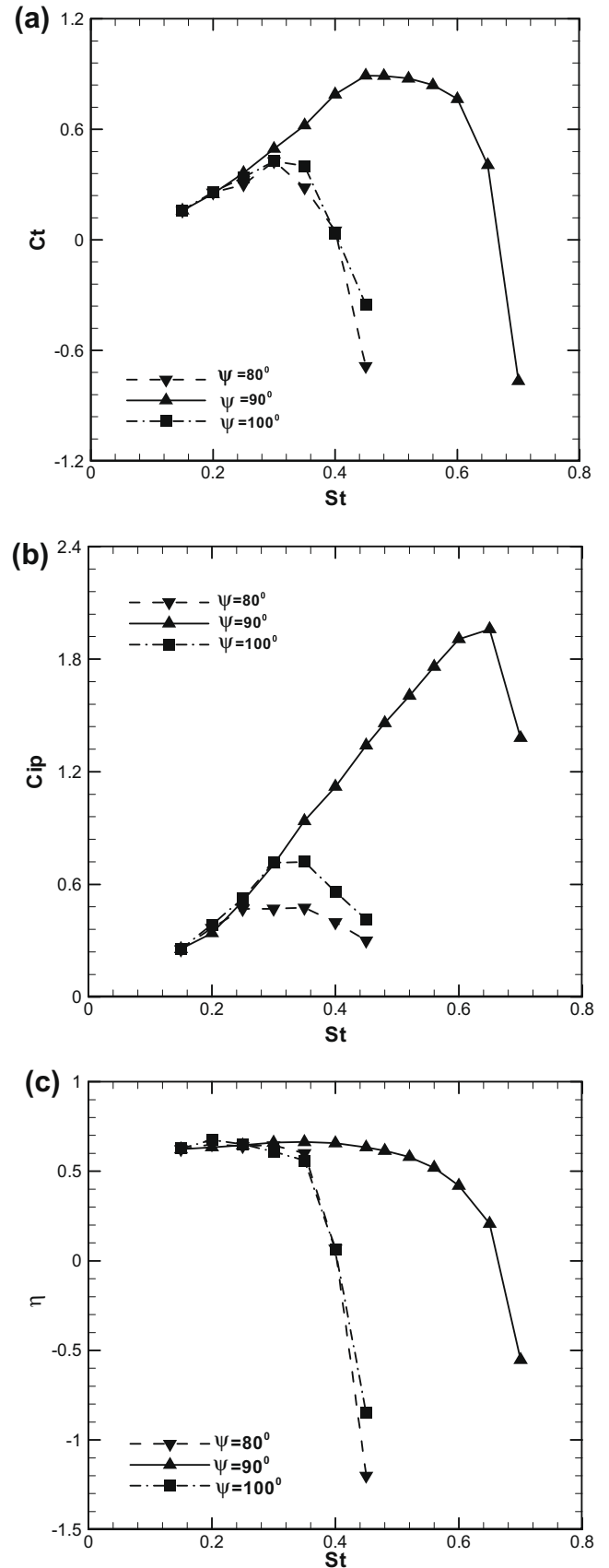


Fig. 6. Effect of ψ on the mean thrust coefficient, power coefficient and propulsion efficiency variation with St for the baseline motion with $h_0 = 1.0$ and $\alpha_{max} = 15^\circ$. (a) Thrust coefficient. (b) Power coefficient. (c) Propulsion efficiency.

tive AOA profile variation with St , in the next section, will show that the much narrower St range for efficient propulsion at $\psi \neq 90^\circ$ than that at $\psi = 90^\circ$ is caused by the severer degradation of the effective AOA profile from harmonic sinusoids at $\psi \neq 90^\circ$.

3.3. Relations between effective angle of attack and oscillating parameters

It is known that the thrust performance is related to the effective angle of attack $\alpha(t)$. From Eq. (11), we can see that $\alpha(t)$ is dependent on the pitching amplitude, phase difference and most significantly on the oscillation frequency St . We discuss the variation of $\alpha(t)$ with St in this section and explore the way to improve thrust performance by changing $\alpha(t)$ profile.

With Eqs. (9) and (10) and definition of St , Eq. (11) can be rewritten as:

$$\alpha(t) = -\arctan(\pi St \cos(\omega t)) + \theta(t) \tag{18}$$

As seen from above expression, for a given plunging amplitude h_0 and phase difference ψ , the effective AOA $\alpha(t)$ is determined by the pitching amplitude θ_0 and St . With a fixed maximum angle of attack α_{max} , the profile of $\alpha(t)$ is solely dependent on St .

For small St , we can approximate arctangent function as

$$\arctan(\pi St \cos(\omega t)) \approx \pi St \cos(\omega t) \tag{19}$$

and thus

$$\alpha(t) \approx -\pi St \cos(\omega t) + \theta_0 \sin(\omega t + \psi) \tag{20}$$

The profile of $\alpha(t)$ for small St is therefore nearly a symmetric or asymmetric simple harmonic form for $\psi = 90^\circ$ or $\psi \neq 90^\circ$, respectively, due to the combination of two harmonic motions of pitching and plunging with the same frequency. However, for a large St , $\alpha(t)$ deviates from simple harmonics with the adding of higher order harmonic components.

The typical variations of $\alpha(t)$ profile with St for $h_0 = 1.0$ and $\alpha_{max} = 15^\circ$ are plotted in Fig. 7a and b for $\psi = 90^\circ$ and $\psi = 80^\circ$, respectively. Given $\psi = 90^\circ$, it is shown that with $St < 0.35$, $\alpha(t)$ generally follows the sinusoidal profile. As St increases to 0.35, $\alpha(t)$ profile becomes flattened in the time range where peak value appears for smaller St . With a further increase of St to 0.45, more than one peak are observed in one period. This becomes more

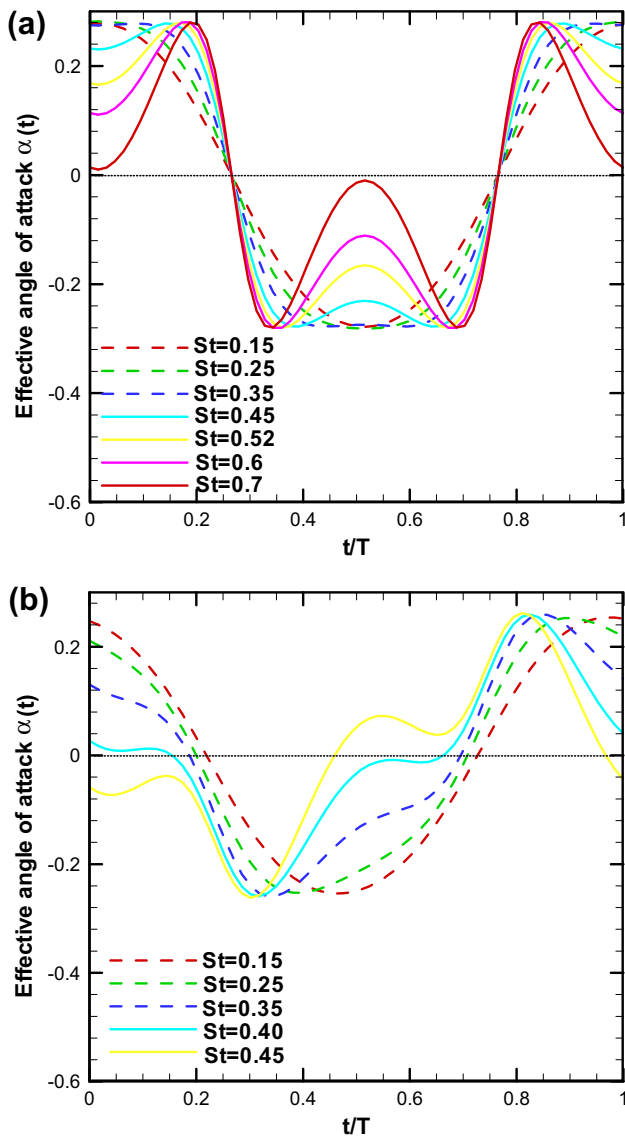


Fig. 7. Variation of $\alpha(t)$ profile versus St for the baseline cases with $h_0 = 1.0$ and $\alpha_{max} = 15^\circ$. (a) $\psi = 90^\circ$ and (b) $\psi = 80^\circ$.

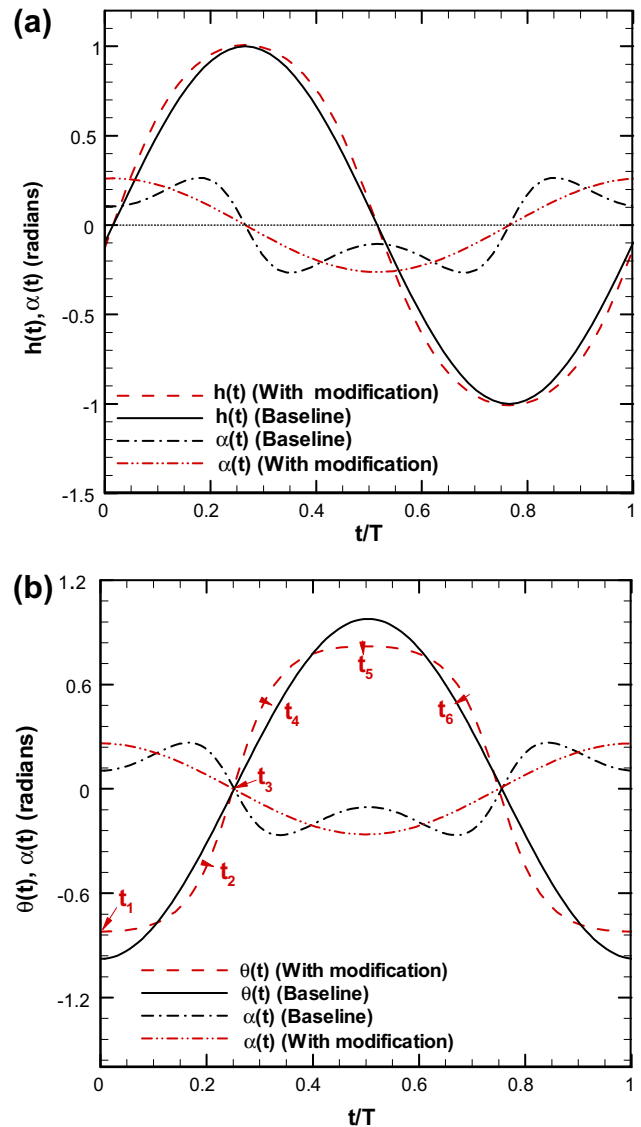


Fig. 8. Variation of instant modified oscillating position and effective AOA in one period for the baseline and modification cases with $h_0 = 1.0$, $\psi = 90^\circ$, $\alpha_{max} = 15^\circ$ and $St = 0.65$. (a) Modified $h(t)$ and the resultant $\alpha(t)$. (b) Modified $\theta(t)$ and the resultant $\alpha(t)$.

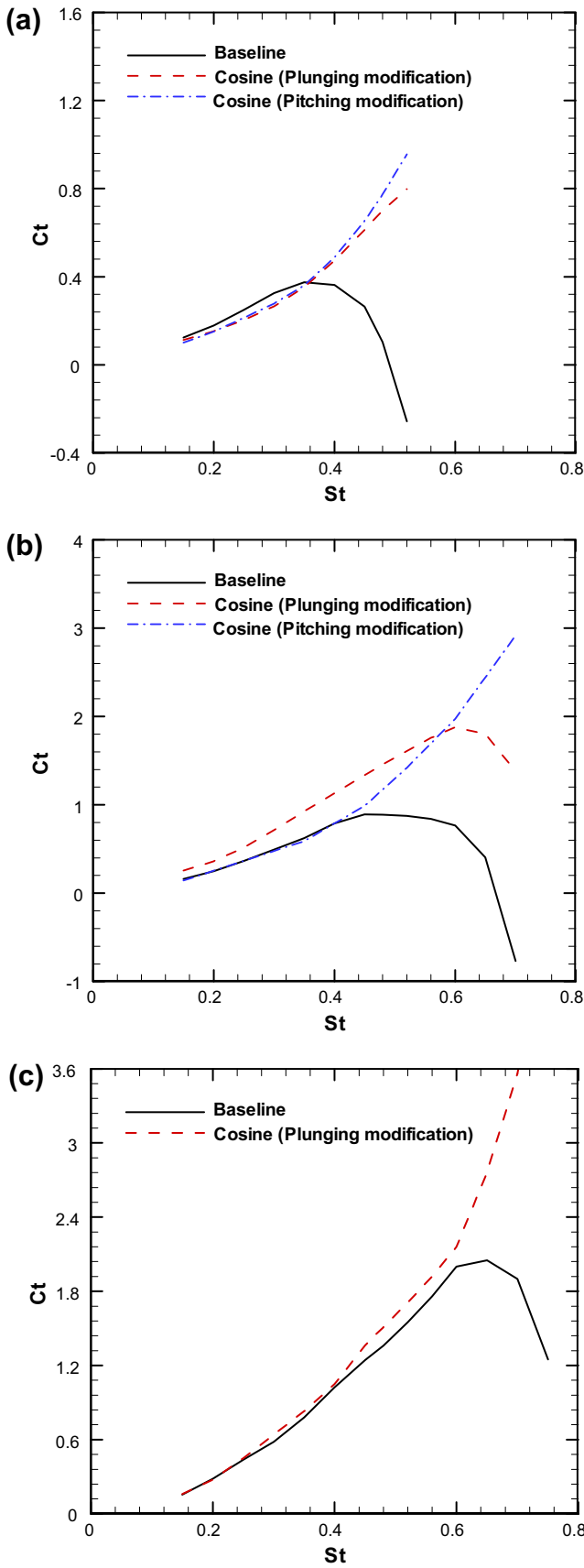


Fig. 9. Effect of the cosine $\alpha(t)$ achieved by modification on the mean thrust coefficient with $h_0 = 1.0$ and $\psi = 90^\circ$. (a) $\alpha_{max} = 10^\circ$, (b) $\alpha_{max} = 15^\circ$, and (c) $\alpha_{max} = 20^\circ$.

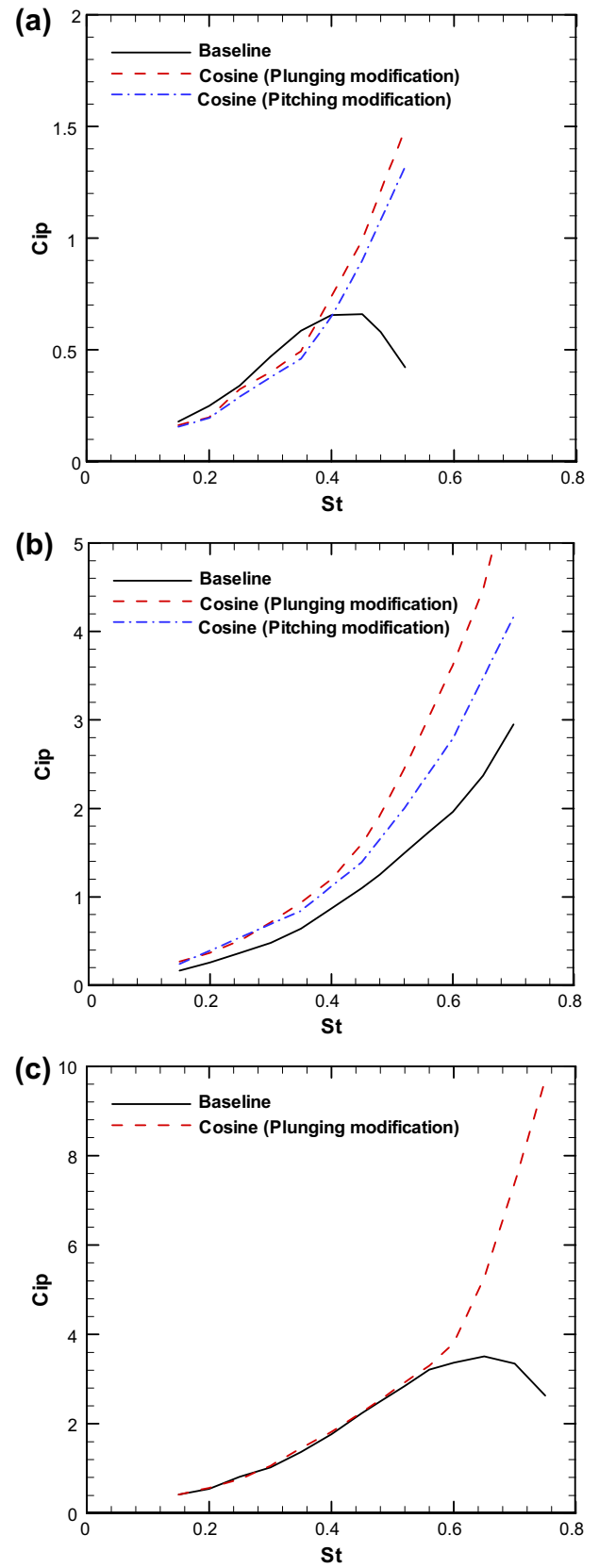


Fig. 10. Effect of cosine $\alpha(t)$ achieved by modification on the power coefficient with $h_0 = 1.0$ and $\psi = 90^\circ$. (a) $\alpha_{max} = 10^\circ$, (b) $\alpha_{max} = 15^\circ$, and (c) $\alpha_{max} = 20^\circ$.

apparent when St further increases to 0.6 and 0.7. Previous experimental work of Read et al. [1] and Hover et al. [2] revealed the

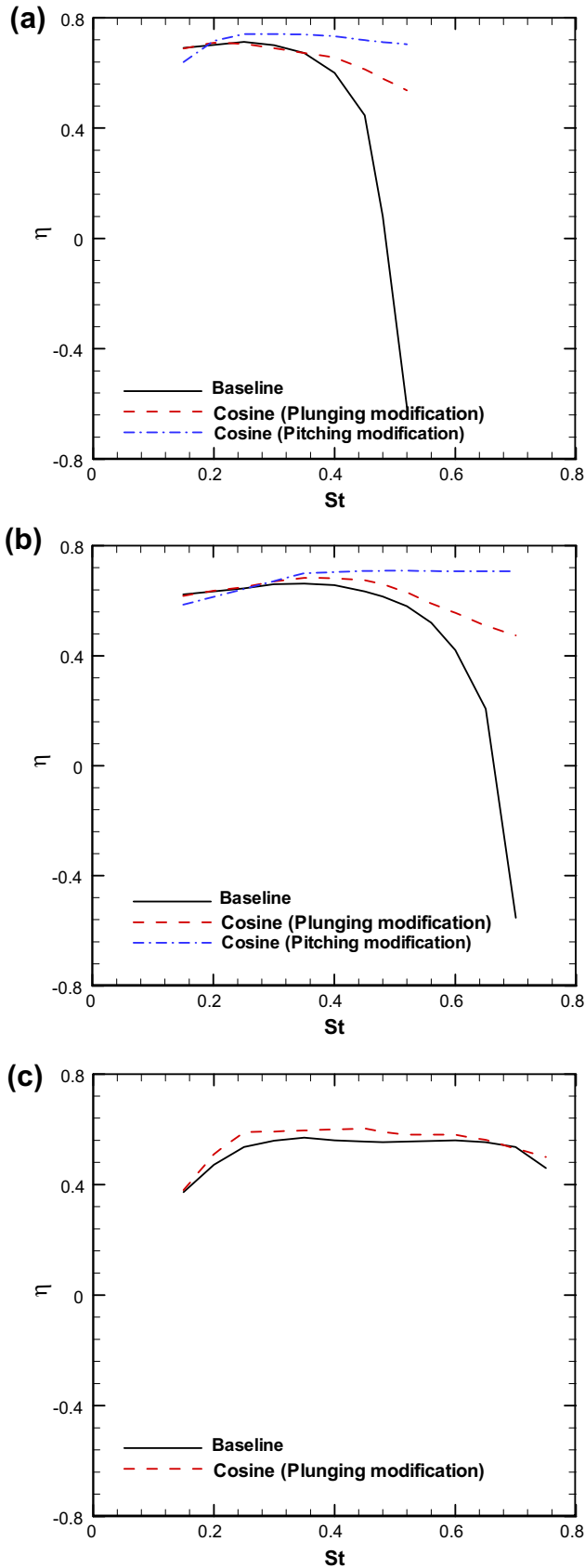


Fig. 11. Effect of cosine $\alpha(t)$ achieved by modification on propulsion efficiency with $h_0 = 1.0$ and $\psi = 90^\circ$. (a) $\alpha_{max} = 10^\circ$, (b) $\alpha_{max} = 15^\circ$, and (c) $\alpha_{max} = 20^\circ$.

similar observation with $\psi = 90^\circ$. For $\psi = 80^\circ$ case shown in Fig. 7b, the breakdown of asymmetric harmonic sinusoidal starts between

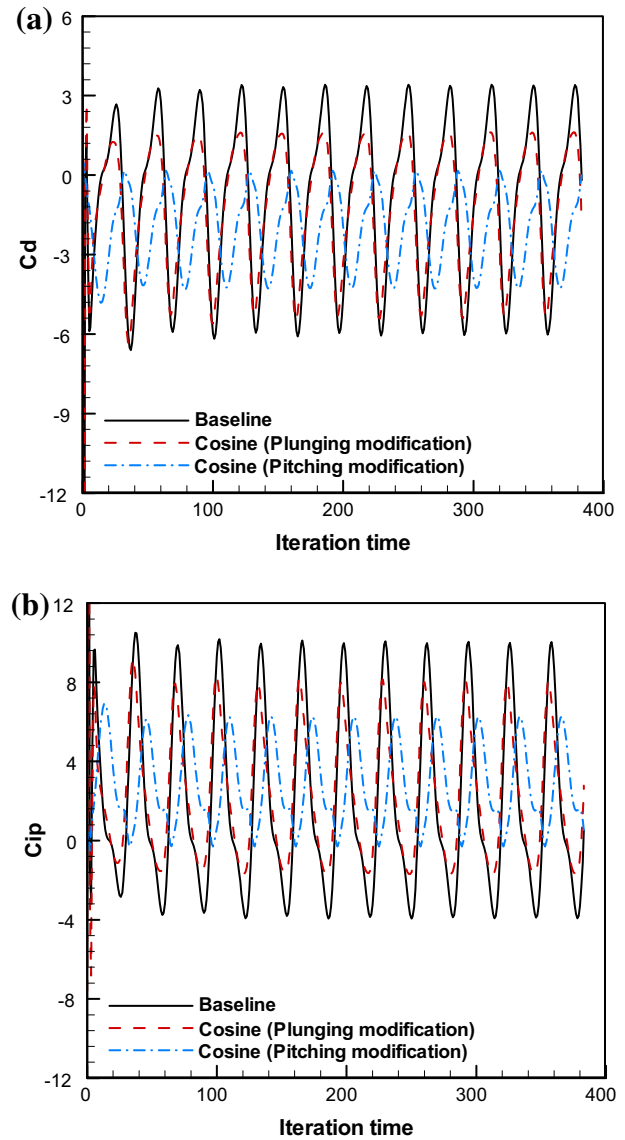


Fig. 12. Comparison of instant drag coefficient, power coefficient variation in one period for the baseline and cosine effective AOA $\alpha(t)$ with $h_0 = 1.0$, $\psi = 90^\circ$, $\alpha_{max} = 15^\circ$ and $St = 0.65$.

$St = 0.25-0.35$, and becomes more and more noticeable with the increasing St . In fact, for $St > 0.3$, the corresponding time-mean thrust coefficient and efficiency dramatically decrease with St as displayed in Fig. 6.

3.4. Results for modified oscillating motions

Since the reduction of thrust coefficient and propulsion efficiency at higher St was found to be influenced by the degradation of effective AOA from simple harmonic profiles, like sinusoids or cosines, it is necessary to make a systematic investigation on how to achieve the high thrust performance by altering the effective AOA profile while maintain the same maximum effective AOA. In this study, a cosine function, which is a typical example of simple harmonics, is utilized for the modified effective AOA profile to examine the improvement of propulsion performance.

3.4.1. Modified pitching/plunging oscillating profile

A representative cosine function of $\alpha(t)$ can be expressed as

$$\alpha(t) = \alpha_{max} \cos(\omega t) \tag{21}$$

To achieve the resultant AOA satisfying above equation, there are two possible approaches by choosing to change the plunging motion or pitching motion. Both approaches are adopted in the current work. We keep one of two motions unchanged from sinusoids and determine the profile of another motion to satisfy the resultant AOA as described by Eq. (21).

In the case of an unchanged sinusoidal *pitching*, the plunging motion is determined as follows. Combine Eqs. (11) and (21), the derivative of plunging motion $\dot{h}(t)$ can be expressed as

$$\frac{\dot{h}(t)}{U_\infty} = \tan(\theta(t) - \alpha(t)) \tag{22}$$

or

$$\dot{h}(t) = U_\infty \tan[\theta_0 \sin(\omega t + \psi) - \alpha_{\max} \cos(\omega t)] \tag{23}$$

When a fixed α_{\max} is considered, the pitching motion is basically maintained unchanged with only its amplitude θ_0 allowed

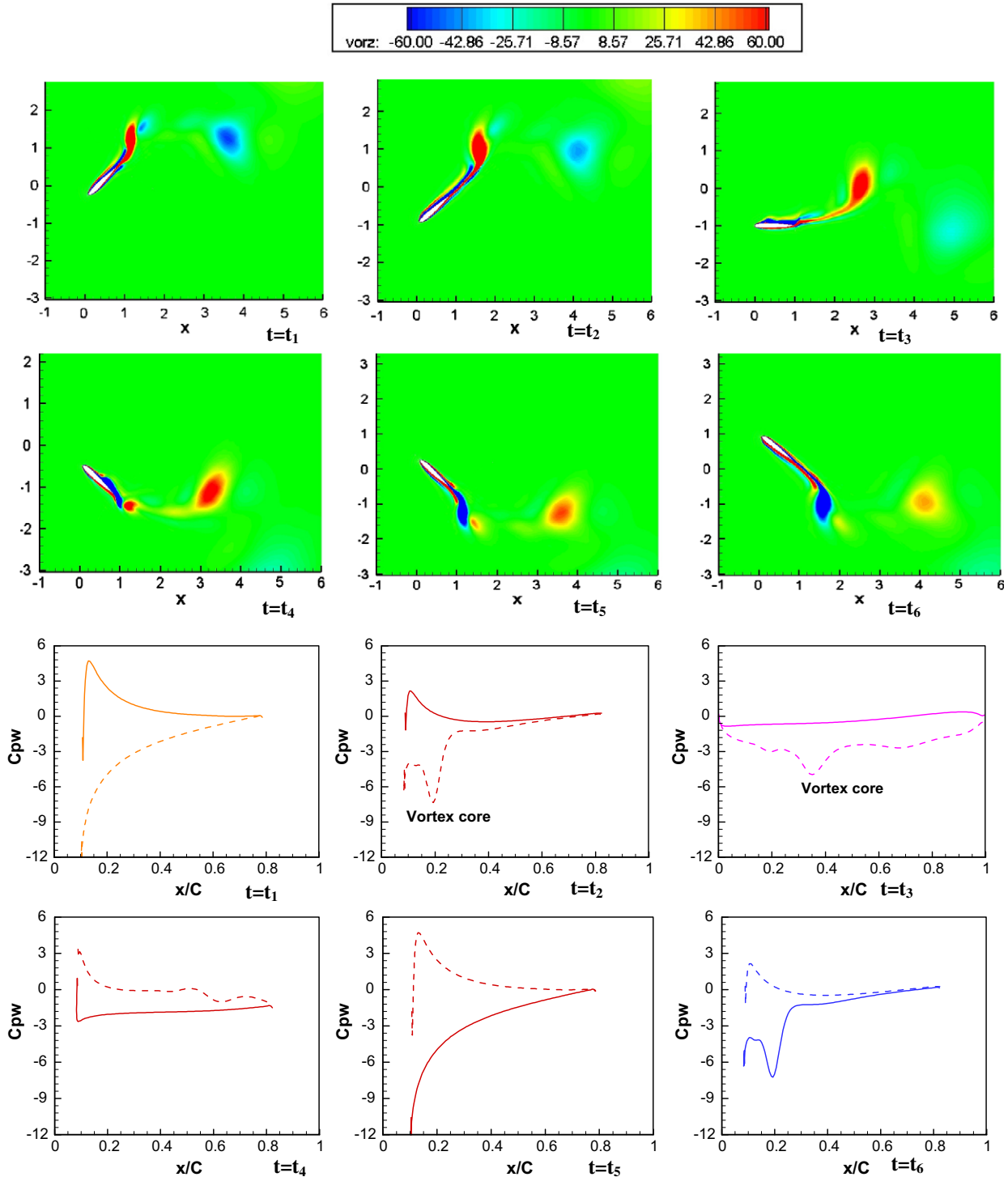


Fig. 13. Vorticity contours and foil surface pressure distribution at six time instants (represented in Fig. 8b) with pitching motion modification for $h_0 = 1.0$, $\psi = 90^\circ$, $\alpha_{\max} = 15^\circ$ and $St = 0.65$. Red: counter clockwise rotating. Blue: clockwise rotating. Solid line: lower wall pressure, dashed line: upper wall pressure. (For interpretation of the references to color in this figure legend, the reader is referred to the web version of this article.)

to be adjusted and the modified plunging motion $h(t)$ is calculated by numerical integration of Eq. (23).

For the case of unchanged sinusoidal plunging, the pitching profile is modified and determined by

$$\theta(t) = \alpha_{\max} \cos(\omega t) + \arctan(\dot{h}(t)/U_{\infty}) \quad (24)$$

Fig. 8a and b shows the variations of modified instantaneous $h(t)$ and $\theta(t)$ computed by Eqs. (23) and (24), respectively. Here the case with $h_0 = 1.0$, $\psi = 90^\circ$, $\alpha_{\max} = 15^\circ$ and $St = 0.65$ is taken as an example to illustrate the modifications and resultant effective AOA obtained by two approaches. As displayed from figures, for an effective AOA of cosine $\alpha(t)$, a slight deviation of $h(t)$ and $\theta(t)$

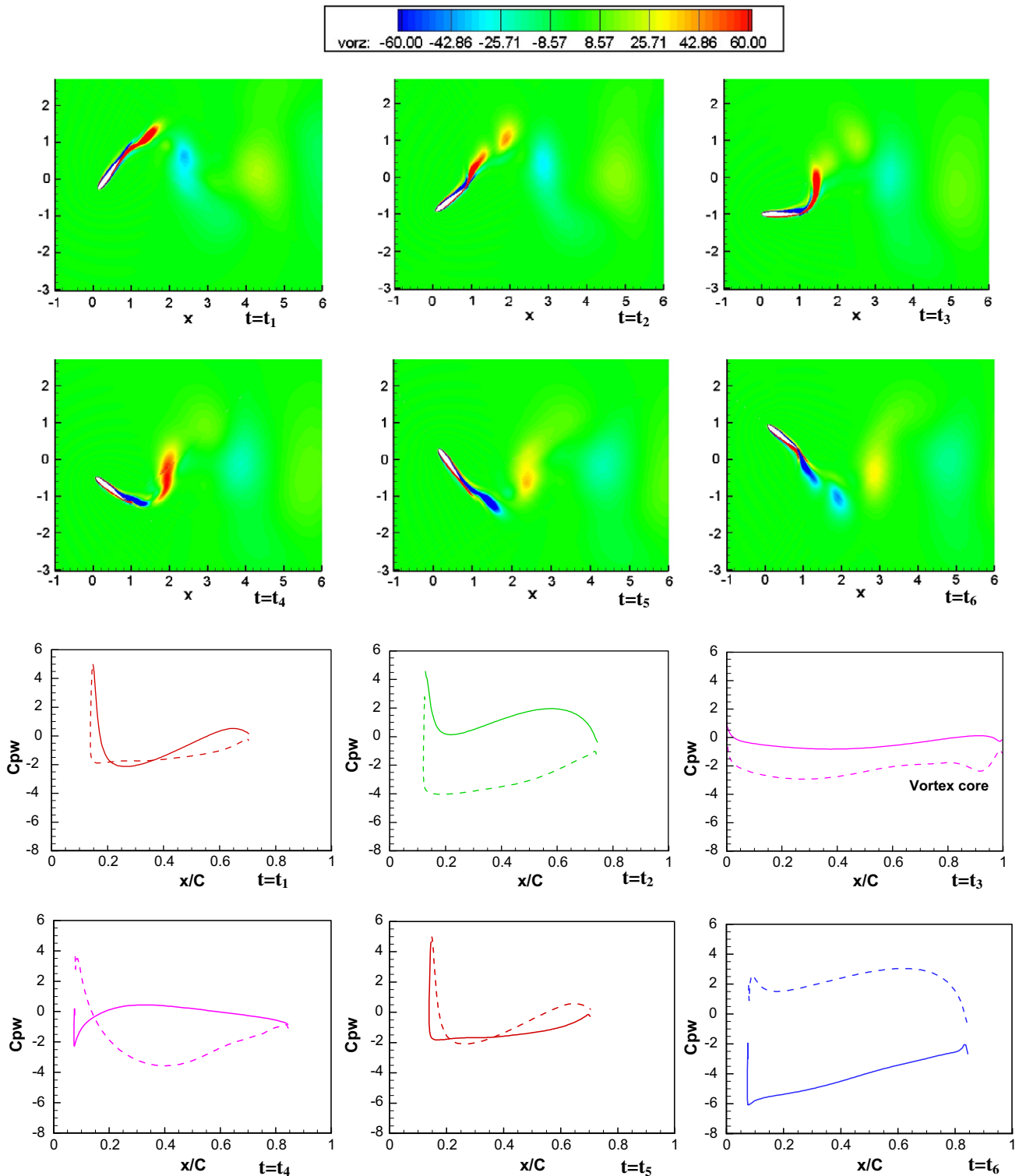


Fig. 14. Vorticity contours and foil surface pressure distribution at six time instants (represented in Fig. 8b) without modification for $h_0 = 1.0$, $\psi = 90^\circ$, $\alpha_{\max} = 15^\circ$ and $St = 0.65$. Red: counter clockwise rotating. Blue: clockwise rotating. Solid line: lower wall pressure, dashed line: upper wall pressure. (For interpretation of the references to color in this figure legend, the reader is referred to the web version of this article.)

from baseline sinusoidal oscillation is observed, which will considerably recover the thrust performance as revealed by the following computed results. With imposed cosine AOA, a much more flattened oscillating profile is found than that with baseline case, which is true for both approaches with modification being applied on either plunging or pitching.

3.4.2. Effect of cosine $\alpha(t)$ at different α_{max}

Figs. 9–11 show the effect of cosine $\alpha(t)$ on the time-mean thrust coefficient, power coefficient and propulsion efficiency for a fixed plunging amplitude of 1.0 and phase difference of 90° with various α_{max} of 10° , 15° and 20° . The modification on the pitching motion is limited to $\alpha_{max} = 10^\circ$ and 15° since with $\alpha_{max} = 20^\circ$, the local Mach numbers in the flow field may exceed 0.3, leading to the breakdown of the near incompressible flow conditions.

It is clear from Fig. 9a–c, for all three α_{max} tested here, the modifications of $\alpha(t)$ eliminate or delay the decrease of thrust coefficient at higher St ($St > 0.4$) compared to the baseline case. In fact, at $\alpha_{max} = 10^\circ$, C_t versus St curves yielded by both modification ap-

proaches present a monotonic increase with St indicating a complete removal of C_t reduction. This is also a case at $\alpha_{max} = 15^\circ$ when the modification is imposed on pitching motion and for $\alpha_{max} = 20^\circ$ with modified plunging. At smaller St , however, computed results of three cases nearly coincide with each other. These results suggest that the modification of AOA takes a positive effect on the propulsion performance at high St while maintains the high performance of baseline motion at small St . In comparison with plunging modification, a slightly higher C_t is obtained by pitching modification at higher St . The power coefficients C_{ip} summarized in Fig. 10a–c revealed that the corresponding C_{ip} with the modification also increases. In general, C_{ip} with modified pitching is lower than that with modified plunging at the same St , leading to the higher propulsion efficiency η as shown in Fig. 11a–c. The improvement of η with modified oscillating is apparent for $\alpha_{max} = 10^\circ$ and $\alpha_{max} = 15^\circ$ though it is not so noticeable for $\alpha_{max} = 20^\circ$.

The comparison of time history on drag coefficient C_d , power coefficient C_{ip} variation in one period for baseline motion and cosine motion is illustrated in Fig. 12a and b with $h_0 = 1.0$, $\psi = 90^\circ$

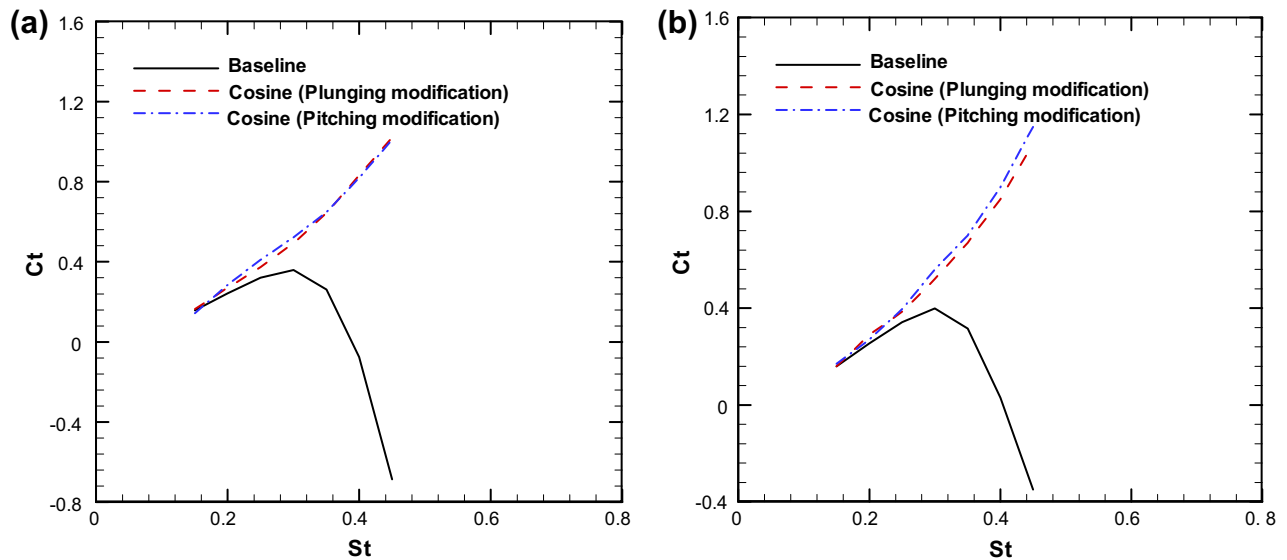


Fig. 15. Comparison of mean thrust coefficient variation with St for the baseline and cosine effective AOA $\alpha(t)$ with $h_0 = 1.0$ and $\alpha_{max} = 15^\circ$. (a) $\psi = 80^\circ$ and (b) $\psi = 100^\circ$.

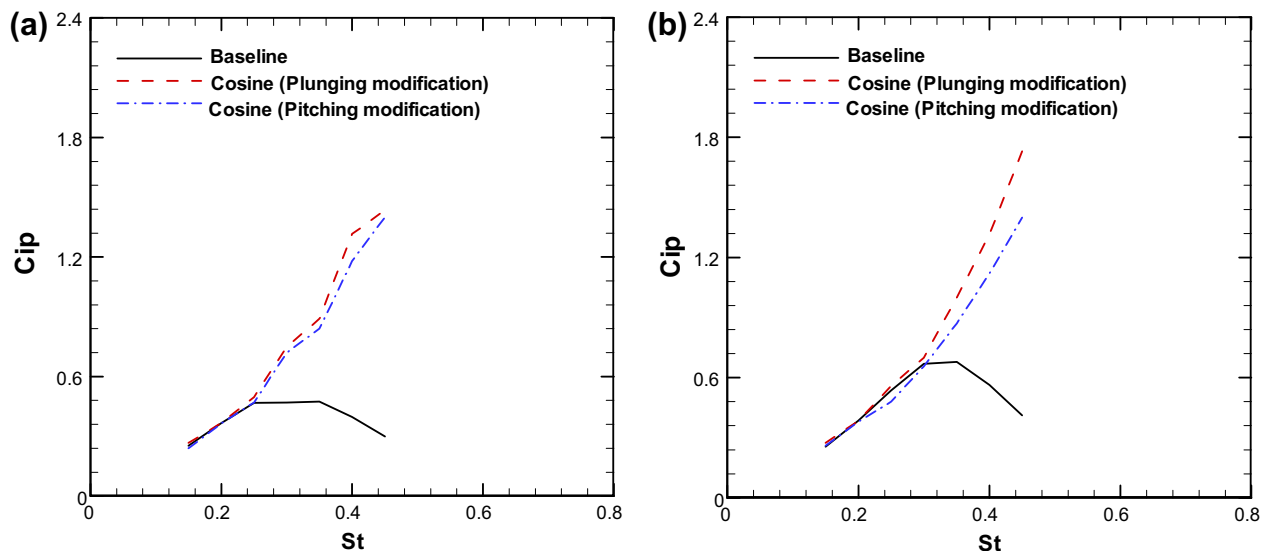


Fig. 16. Comparison of mean power coefficient variation with St for the baseline and cosine effective AOA $\alpha(t)$ with $h_0 = 1.0$ and $\alpha_{max} = 15^\circ$. (a) $\psi = 80^\circ$ and (b) $\psi = 100^\circ$.

and $\alpha_{\max} = 15^\circ$ at $St = 0.65$. With the modification, the amplitude of oscillating C_d decreases and the variation is more concentrated to the negative zone resulting in an increased mean thrust ($-C_d$). Power coefficient results in Fig. 12b show the similar trend with the magnitude of C_{ip} decreasing due to the modification.

Figs. 13 and 14 illustrate the vorticity contours and corresponding pressure distributions at six time instants as shown in Fig. 8b during a cycle for baseline and modified motions. Here, a finer grid with the size of 513×129 is used to capture the vortex structure. For brevity, we only examine the pitching modification instead of presenting two modification approaches. From the two figures, it can be seen that the vortex evolution plays an important role in the thrust production. The vortex development in both cases shows distinct difference. Although the vortices for two cases shed in pairs and the reversed Von Karman vortex pattern in the wake is observed, the vortices from the modified motion are much stronger than those from the baseline motion and resulting in the significant enhancement of the thrust production. Furthermore, the evolution of the stronger leading-edge vortex (LEV) in the modified

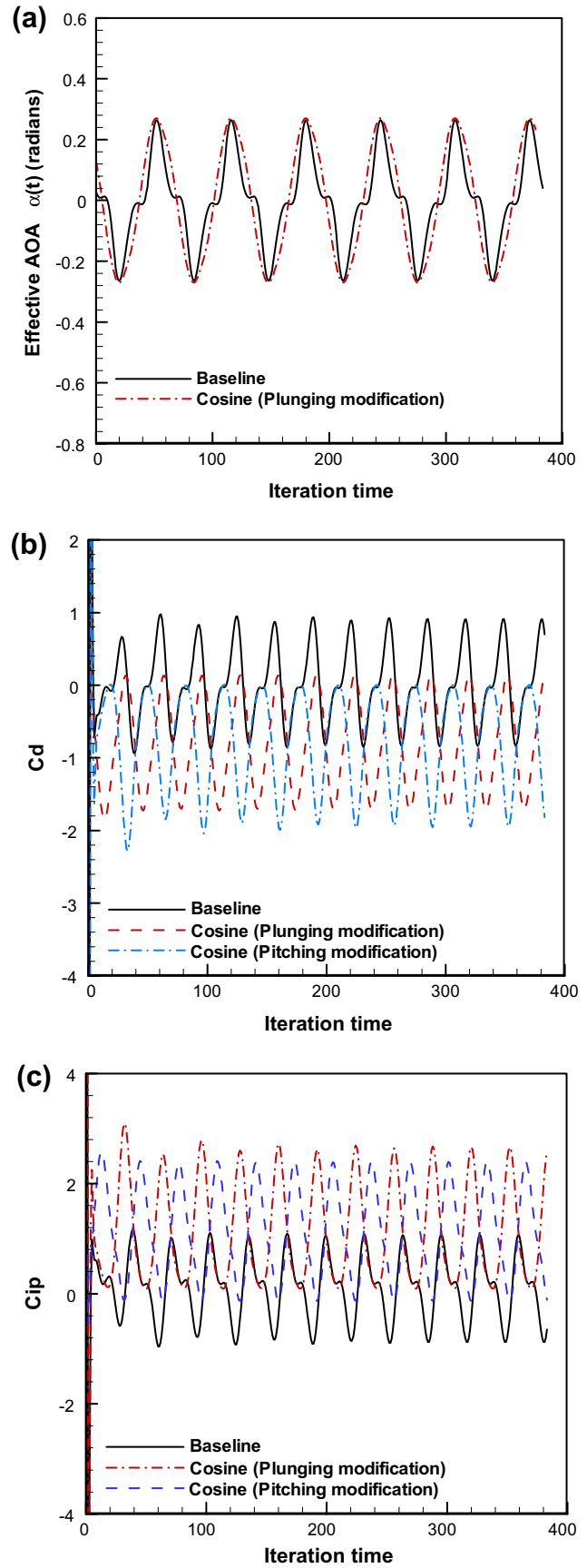
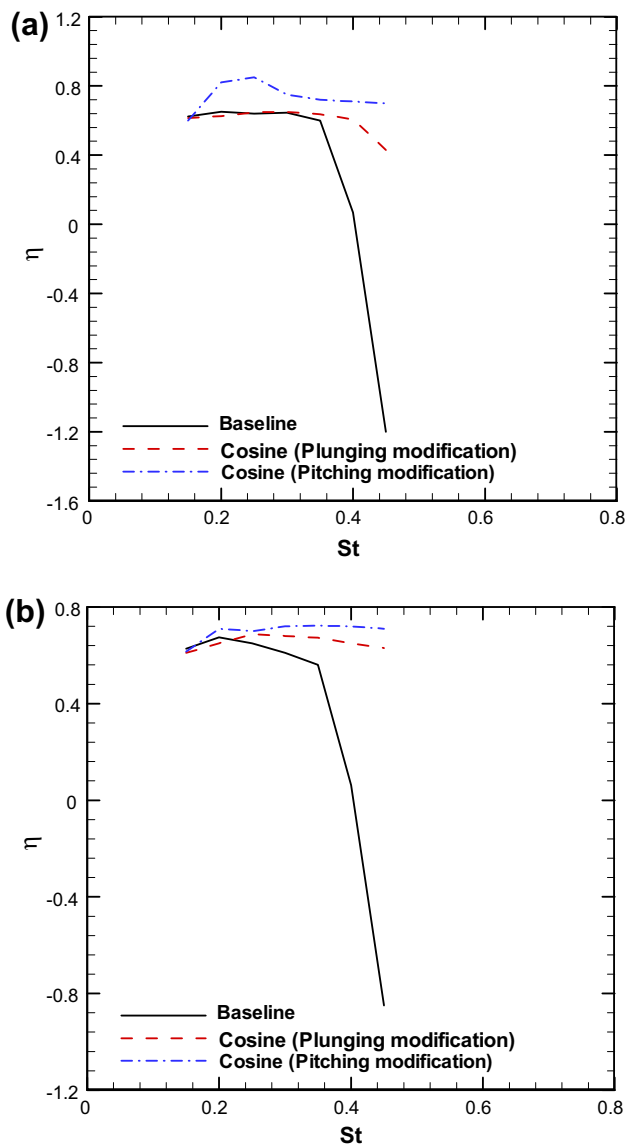


Fig. 17. Comparison of mean thrust propulsion efficiency variation with St for the baseline and cosine effective AOA $\alpha(t)$ with $h_0 = 1.0$ and $\alpha_{\max} = 15^\circ$. (a) $\psi = 80^\circ$ and (b) $\psi = 100^\circ$.

Fig. 18. Time history for instant effective AOA, drag coefficient and power coefficient for $h_0 = 1.0$, $\psi = 80^\circ$, $\alpha_{\max} = 15^\circ$ and $St = 0.35$. (a) Effective AOA. (b) Drag coefficient. (c) Power coefficient.

case also contributes to the thrust enhancement. As shown in Fig. 13, we can see that when the foil with modified motion moves to its maximum negative pitching position (nose-down) at t_1 , an LEV emerges near the leading edge on the upper surface of foil. The vortex creates a very low pressure zone near the foil head thus enhancing the thrust. Afterwards, the LEV grows in size and travels downstream as the foil heads up at t_2 and further develops reaching the zero instant pitching angle at time t_3 . The corresponding wall pressure distribution at t_2 and t_3 clearly reflect the downstream movement of low pressure zone along the upper surface. At t_4 , the foil pitches with nose-up direction, the vortex moves to near trailing edge. As the foil continues moving nose up to maximum pitching angle at t_5 , the vortex is shed into the wake and eventually loses their strength. The foil starts pitching down after time instant t_5 and LEV appears on the lower surface of foil as seen from corresponding pressure distribution at t_5 and t_6 . One strong clockwise rotating vortex is shedding adjacent of the foil with one counter clockwise rotating vortex appearing further downstream. In contrast to the modified case, the LEV development in the baseline case is too weak to be observed clearly as shown in Fig. 14 and thus does not help much in its thrust production.

3.4.3. Effect of cosine $\alpha(t)$ at different ψ

The investigation of cosine $\alpha(t)$ effect on thrust generation is further extended to different phase angles ψ . Figs. 15–17 show how $\alpha(t)$ affects the time-mean thrust coefficient, power coefficient and propulsion efficiency for $\psi = 80^\circ$ and $\psi = 100^\circ$ with $h_0 = 1.0$ and $\alpha_{\max} = 15^\circ$. In the range of $0.1 < St < 0.25$, where C_t and C_{ip} increase with St for both $\psi = 80^\circ$ and $\psi = 100^\circ$, no significant difference on thrust coefficient or power coefficient is observed between the baseline and the cosine $\alpha(t)$. This is consistent with the asymmetric simple harmonic AOA profile at low St shown in Fig. 7b. With further increasing St , thrust coefficient C_t and power coefficient C_{ip} with modification continue increasing with St while both of them for baseline cases present a fast decay with St . The improvement with modification is considerable at this St range where the severe degradation of AOA profile displayed in Fig. 7b is removed with imposed cosine profile. In fact, as seen from Figs. 15a and b, with baseline motions, when St is more than 0.4, the fast decay of C_t after an extreme point leads to the occurrence of the negative C_t representing the drag producing. The modified effective AOA removes that extreme point and C_t maintains the monotonic growth with St . Thus, with the modification, the flow changes from drag producing to thrust producing at $St > 0.4$. The differences on C_t from modified pitching and plunging are very subtle within entire tested St range and for $\psi = 80^\circ$ and $\psi = 100^\circ$ cases. The C_{ip} with modified plunging is larger than the counterpart of modified pitching leading to the lower efficiency especially at higher St as shown in Fig. 17a and b. Compared to $\psi = 90^\circ$ case displayed in Fig. 9b, it is noteworthy that the improvement on thrust coefficient achieved by the cosine $\alpha(t)$ is more efficient for the phase difference $\psi \neq 90^\circ$ than that for $\psi = 90^\circ$ in a sense that the declining of C_t with baseline motions is completely eliminated with modified motions imposed on plunging.

The time history for instantaneous parameters like effective AOA, thrust (drag) coefficient and efficiency variation are plotted in Fig. 18a–c for $h_0 = 1.0$, $\alpha_{\max} = 15^\circ$ and $\psi = 80^\circ$ at $St = 0.35$. Significant improvement of thrust coefficient, i.e., $-C_d$, for the cosine $\alpha(t)$ is revealed in Fig. 17b although the input power is also increased slightly as shown in Fig. 17c.

4. Conclusions

We investigate numerically the effect of effective angle of attack profile on the propulsion performance of an oscillating NACA0012

foil. The harmonic cosine form of effective AOA profile achieved by modifying the plunging or pitching motion is studied over a wide range of Strouhal numbers St , three different maximum effective AOA α_{\max} and different phase difference between pitching and plunging ψ .

For the baseline motion, with a relatively high St , the AOA profile deviates from simple harmonics, which causes the degradation of thrust coefficient and propulsion efficient. Significant improvement on thrust coefficient and propulsion efficiency at high St can be achieved when the effective AOA profile is maintained to be a harmonic cosine function by controlling the plunging or pitching motions of the foil. The improvement is more apparent for the phase difference $\psi \neq 90^\circ$ than that for $\psi = 90^\circ$ since the non-harmonic AOA profile appears at smaller St with $\psi \neq 90^\circ$. As a result, a minor modification on either the pitching or plunging motion from sinusoids effectively extends the St range in which the high thrust performance occurs. At small St , the modification effect is not remarkable and propulsion performance remains almost the same as that for the baseline motion. In addition, comparison between two modification approaches reveal that the modification imposed on the pitching motion achieves much better improvement than that on the plunging adjustment. Detailed examination on the wake structure and the foil surface pressure distribution reveals a stronger reversed Von Karman vortex structure generated with the cosine function, associated with the appearance of significant leading-edge vortex, which leads to an effective prevention of the fast decay on thrust and efficiency at high St .

Acknowledgments

The authors are grateful to the reviewers whose comments have helped us improve the manuscript considerably.

References

- [1] Read DA, Hover FS, Triantafyllou MS. Forces on oscillating foils for propulsion and maneuvering. *J Fluids Struct* 2003;17:163–83.
- [2] Hover FS, Haugsdal O, Triantafyllou MS. Effect of angle of attack profiles in flapping foil propulsion. *J Fluids Struct* 2004;19:37–47.
- [3] Anderson JM. Vorticity control for efficient propulsion. PhD Thesis. Massachusetts Institute of Technology and Woods Hole Oceanographic Institution; 1996.
- [4] Anderson JM, Streitlien K, Barrett DS, Triantafyllou MS. Oscillating foils of high propulsive efficiency. *J Fluid Mech* 1998;360:41–72.
- [5] Lewin GC, Haj-Hariri H. Modelling thrust generation of a two-dimensional heaving airfoil in a viscous flow. *J Fluid Mech* 2003;492:339–62.
- [6] Tuncer IH, Platzer MF. Computational study of flapping airfoil aerodynamics. *J Aircraft* 2000;37:514–20.
- [7] Young J, Lai JCS. Oscillation frequency and amplitude effects on the wake of a plunging airfoil. *AIAA J* 2004;42:2042–52.
- [8] Lai JCS, Platzer MF. Jet characteristics of a plunging airfoil. *AIAA J* 1999;37:1529–37.
- [9] Isogai K, Shinmoto Y, Watanabe Y. Effects of dynamic stall on propulsive efficiency and thrust of flapping airfoil. *AIAA J* 1999;37:1145–51.
- [10] Yang S, Luo S, Liu F, Tsai H-M. Computation of the flows over flapping airfoil by the Euler equations. *AIAA Paper* 2005-1404; January 2005.
- [11] Koochesfahani MM. Vortical patterns in the wake of an oscillating airfoil. *AIAA J* 1989;27(9):1200–5.
- [12] Sarkar S, Venkatraman K. Numerical simulation of thrust generating flow past a pitching airfoil. *Comput Fluids* 2006;35:16–42.
- [13] Sarkar S, Venkatraman K. Numerical simulation of incompressible viscous flow past a heaving airfoil. *Int J Numer Meth Fluids* 2006;51:1–29.
- [14] Xiao Q, Tsai HM, Papamoschou D. Numerical investigation of supersonic nozzle flow separation. *AIAA J* 2007;45:532–41.
- [15] Xiao Q, Tsai HM, Liu F. A numerical study of transonic buffet on a supercritical airfoil. *AIAA J* 2006;44(3):620–8.
- [16] Xiao Q, Liao W. Numerical investigation of angle of attack profile on propulsion performance of an oscillating foil. *AIAA Paper* 2009-725; 2009.
- [17] Xiao Q, Liao W. Numerical study of asymmetric effect on pitching foil. *Int J Mod Phys C* 2009;20:1663–80.
- [18] Jameson A, Schmitt W, Turkel E. Numerical solutions of the Euler equations by finite volume methods using Runge–Kutta time stepping schemes. *AIAA Paper* 81-1259; January 1981.
- [19] Jameson A. Time-dependent calculations using multigrid with applications to unsteady flows past airfoils and wings. *AIAA Paper* 1991-1596; June 1991.

- [20] Jones KD, Platzer MF. Numerical computation of flapping-wing propulsion and power extraction. AIAA Paper 97-0826; 1997.
- [21] Liu H, Kawachi K. A numerical study of undulatory swimming. *J Computat Phys* 1999;155(2):223–47.
- [22] Ramamurti R, Sandberg W. Simulation of flow about flapping airfoils using finite element incompressible flow solver. *AIAA J* 2001;39(2):253–60.
- [23] Young J, Lai JCS. Oscillation frequency and amplitude effects on the wake of a plunging airfoil. *AIAA J* 2004;42(10):2042–52.
- [24] Liao W, Cai J, Tsai HM. A multigrid overset grid flow solver with implicit hole cutting method. *Comput Meth Appl Mech Eng* 2007;196:1701–15.